

## A Perspective on Computational Aerothermodynamics at NASA

Peter A. Gnoffo<sup>1</sup>

<sup>1</sup>NASA Langley Research Center  
Hampton, Virginia, 23681, USA

### Abstract

The evolving role of computational aerothermodynamics (CA) within NASA over the past 20 years is reviewed. The presentation highlights contributions to understanding the Space Shuttle pitching moment anomaly observed in the first shuttle flight, prediction of a static instability for Mars Pathfinder, and the use of CA for damage assessment in post-Columbia mission-support. In the view forward, several current challenges in computational fluid dynamics and aerothermodynamics for hypersonic vehicle applications are discussed. Example simulations are presented to illustrate capabilities and limitations. Opportunities to advance the state-of-art in algorithms, grid generation and adaptation, and code validation are identified.

### Introduction

Computational fluid dynamics (CFD) is the numerical simulation of flowfields through the approximate solution of the governing partial differential equations for mass, momentum, and energy conservation coupled with the appropriate relations for thermodynamic and transport properties. Aerothermodynamics is the branch of fluid dynamics that focuses on the effects of thermodynamic and transport models on aerodynamics and heating. It is especially focused on conditions of hypersonic velocities where the energy content and exchange between kinetic, internal, and chemical modes in the flow precludes the otherwise common use of calorically perfect gas assumptions. Computational aerothermodynamics is therefore defined in exactly the same manner as CFD, with the added emphasis that high temperature gas effects on pressure, skin friction, and heat transfer are included in the numerical simulation. The fundamental role of computational aerothermodynamics is the simulation of aerodynamic forces and heating for external and internal high speed flows. Reference [21] presents a review of recent applications for access to space and planetary missions.

The evolving capabilities of computational aerothermodynamic (CA) simulation and its role in various NASA programs is reviewed. The review provides context for discussion of new research and development in CA. Emphasis is placed on the more recent role of finite-volume, (pseudo) time-dependent Navier-Stokes solvers using upwind discretizations to capture strong shocks. Within NASA, these schemes began displacing conventional discretizations (MacCormack's method or central difference methods with second-order implicit and fourth-order explicit smoothing and shock fitting) in the late 1980's. Space-marching, Parabolized Navier-Stokes methods were supplanted as well when more powerful computers became available such that the inherent restrictions to attached flow and spatial step size no longer had to be endured. It is interesting to note that the predominant algorithms of the 1970's for heating analyses (viscous-shock-layer (VSL) and boundary-layer equation solutions tied to inviscid surface pressure distributions are seeing a resurgence as engineering tools to provide quick running, multiphysics simulations.

The first three sections of this paper highlight examples where CA simulations offered unique insight to an important prob-

lem within NASA regarding hypersonic flight environment. In the first two examples - a shuttle orbiter body-flap anomaly on STS-1 and a Mars Pathfinder static instability - CA simulations demonstrated that subtle changes in gas chemistry can have large effects on aerodynamics. Furthermore, the ability of CA to quantify the distribution of pressure and shear provided the best understanding of the integrated effects measured in flight or ground-based tests. In the third example - Columbia accident investigation - CA provided data early in the investigation to establish mass and energy flux into the wing as a function of breach size and local boundary-layer thickness as well as the extreme heating environments on the downstream edge of the breach. These breach simulations demonstrated that CA could respond in a timely manner to analyze damage to the outer-mold-line and evolved to inclusion of CA within the Damage Assessment Team that stands by for support in every mission today. All of these examples served to enhance the perception of CA as an ever stronger tool for understanding the environment of a hypersonic vehicle.

Even with these and other successes much advance to the state-of-art (SOA) is still required. A brief review of current SOA follows in the next section. Too often, a new capability is inextricably hardwired throughout a single code or is demonstrated for an idealized test problem but is never matured for routine use by the larger community. A reference to SOA herein refers to capabilities in codes accepted by project offices for vehicle design. A recent simulation of a flexible ballute - deployable aerobrake - is provided to show specific advances required in both numerical and physical model capability. It provides context to say this is what we can do now and this is what we still need to be able to do. CA is a very broad field and because of the difficulty in obtaining data at hypervelocity conditions in ground-based facilities it becomes an especially important tool for establishing aerothermodynamic environments. It is hoped that these examples of CA evolution within NASA provide helpful perspective for researchers entering this field.

### Pitching Moment Anomaly in STS-1 (Reference [37])

On the entry phase of its first flight in April 1981, designated Space Transportation System (STS)-1, the Shuttle Orbiter exhibited hypersonic pitching moment characteristics significantly different from those derived from preflight predictions. The vehicle's bodyflap had to be deflected to an angle over twice that predicted prior to the flight in order to maintain trim. The aerodynamic performance characteristics of the Orbiter had been determined by extensive testing in ground-based facilities. Because real-gas effects could not be fully simulated in ground-based facilities, some analytical assessments were made for real-gas effects on Orbiter aerodynamics. These analytical assessments of real-gas effects were not viewed with much confidence (pre-1981), and thus they were applied to the uncertainty in the aerodynamics of the vehicle rather than to its expected aerodynamic performance. Because of the large uncertainty assigned to these predicted aerodynamics in the hypersonic speed range, ample control power was built into the system to overcome the anomaly in the flight pitching moment.

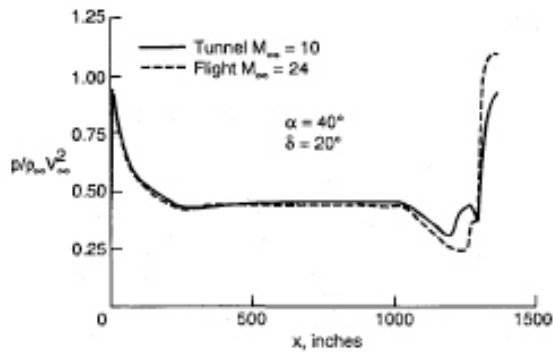


Figure 1: Computed windward centerline pressure distribution.

Still, the large bodyflap deflection required to trim the vehicle raised concerns for the structural and thermal integrity of the bodyflap.

The inability to predict the hypersonic pitching-moment characteristics of the Orbiter, despite extensive wind-tunnel testing, was a fundamental concern. The pitching-moment anomaly had been attributed to a number of phenomena including viscous effects, diminished bodyflap effectiveness, Mach number effects, and real-gas effects. Contemporary SOA analyses either did not include gas chemistry nor have the ability to predict separated flow in front of a deflected body-flap [36] or were forced to make approximations to vehicle geometry and gas chemistry due to limitations imposed by computer hardware [23]. The shuttle aerodynamic databook was corrected based on flight data. Still, a more definitive answer from CA required increased sophistication and robustness of flow solvers and a several-order-of-magnitude increase in computer power available in the early 1990's in order to better define the Orbiter configuration and to utilize proper gas chemistry models.

CA simulations on a modified Orbiter configuration were used to establish that high-temperature gas effects in a seven-species air model account for the different aerodynamic characteristics of the Orbiter at wind tunnel and flight conditions. The aerodynamics of the basic body and the bodyflap were investigated independently, and it was shown that most of the increment can be attributed to the basic body. The bodyflap was shown to be as much as 1.5 times more effective in flight than in the wind tunnel, which contradicts assertions that the Orbiter pitching-moment "anomaly" was caused by reduced bodyflap effectiveness in flight. In fact, had the bodyflap exhibited the same effectiveness in flight as in the wind tunnel, the vehicle may not have trimmed at all. All evidence from CA analyses led to the conclusion that the so-called "pitching-moment anomaly" that occurred on STS-1 was caused by the inability of perfect-gas ground-based facilities to simulate the real-gas chemistry encountered by the vehicle in hypersonic flight. The aerodynamic increments between wind-tunnel and flight conditions in Figure 1 is attributable to a relatively small pressure differential acting on an expansion surface at the aft end of the vehicle, which has a very large surface area. The net effect of this difference on pitching moment is shown in Figure 2 in which the flight simulation (closed circles) is in agreement with derived flight data (open squares).

Notable restrictions in the simulation from that period included a post-processing approximation to include effects of elevelon gaps and near wake flow because the complexity of resolving these features strained available resources. As it was, the nose to trailing edge simulation was implemented in a block march-

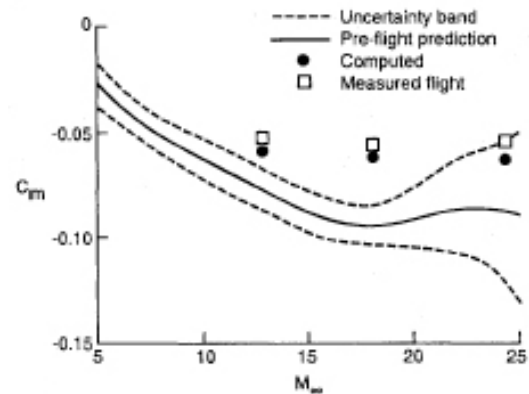


Figure 2: Comparison of predicted, measured, and computed pitching moment coefficient over the hypersonic portion of the STS-2 entry trajectory.

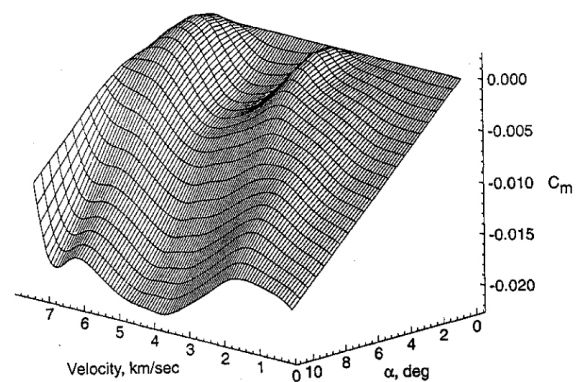


Figure 3: Pitching moment coefficient vs velocity and angle of attack for Mars Pathfinder.

ing mode that required more user intervention in selection of sub-domains that is no longer required in equivalent simulations today.

#### Static Instability in Mars Pathfinder (References [20, 8, 18])

CA was used to develop the Mars Pathfinder aerodynamic databook in 1995. It leveraged some ground-based aerodynamic data from the earlier Viking tests (same forebody shape) but it needed to focus on angle-of-attack near zero because Pathfinder was spin-stabilized whereas Viking flew at 11 degrees with reaction control system jets. As the matrix of simulations was being completed a surprising result was obtained in the pitching moment coefficient,  $C_m$ . At small angles of attack  $C_m$  was positive (and consequently  $C_{m,\alpha}$  was positive and destabilizing) at two regions in velocity space ( $\approx 7.0$  km/s and  $\approx 3.5$  km/s) as evident in the two folds in Figure 3. An investigation was launched [20] to explain this behavior and ask what happens at these velocities that is not in play at other velocities.

The major conclusions of that study showed that as the Mars Pathfinder probe descended through the Martian atmosphere the minimum value of the postshock effective  $\gamma$  (ratio of specific heats) first decreased from frozen gas chemistry values ( $\approx 1.333$ ) to equilibrium values (1.094) corresponding to a velocity of 4.86 km/s. As the probe continued to decelerate through an equilibrium postshock gas chemistry regime, the value of  $\gamma$  increased again, until reaching its perfect-gas value of  $\approx 1.333$  at parachute deployment (0.42 km/s). At small angles of attack ( $\alpha < 5$  deg) the sonic line location shifts from

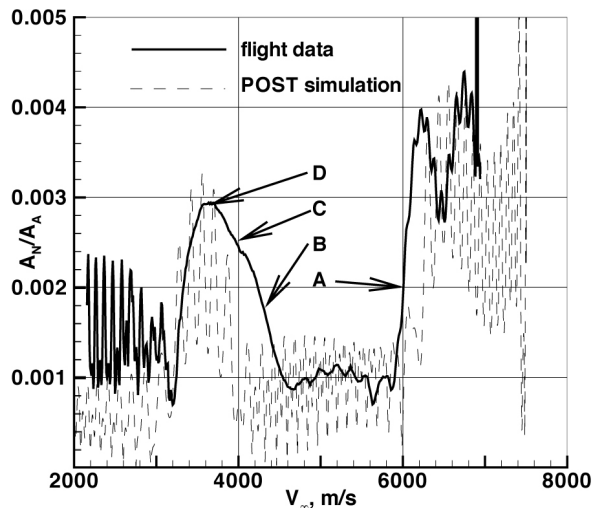


Figure 4: Comparison of  $A_N/A_A$  as measured in flight and as simulated with the POST code for the reconstructed atmosphere using the CFD derived database for the aerodynamic coefficients for Mars Pathfinder.

the shoulder to the nose cap and back again on the leeside symmetry plane because of the change in  $\gamma$  for the cone half-angle of 70 deg. The sonic line shift is accommodated by a bubble of subsonic flow behind the shock that grows to connect the corner to the spherical nose cap.

Pressure distributions on the cone frustum approaching the shoulder tend to be very flat when the sonic line sits forward over the spherical nose. Effects of the expansion over the shoulder can only be communicated upstream through the subsonic portion of the boundary layer. In contrast, pressure distributions on the cone frustum approaching the shoulder tend to be more rounded when the sonic line sits on the shoulder, exhibiting a more pronounced influence of the expansion on the upstream flow. In general, windside pressures exceed leeside pressures on the cone frustum, producing a stabilizing moment that pitches the probe back to zero angle of attack. However, the behavior of the pressure distribution in the vicinity of the shoulder significantly influences the pitching-moment coefficient because of the relatively larger moment arms and surface area at the edge of the probe as compared to the inboard nose and frustum regions. For the Mars Pathfinder probe at 2-deg angle of attack, the flat, leeside pressures approaching the shoulder (when the sonic line sits over the nose) can exceed the rounded windside pressures approaching the shoulder (when the sonic line sits over the shoulder). The net effect of this crossover distribution near the shoulder tends to pitch the probe to higher angles of attack. The overall balance (crossover-point location) is sensitive to both freestream conditions and the gas chemistry.

Therefore conditions for a positive, destabilizing moment coefficient derivative occur twice in the Mars Pathfinder mission. The first occurrence ( $7.5 > V_\infty > 6.5$  km/s,  $51 > h > 37$  km, vicinity of peak heating for this trajectory) results from the translation in the sonic-line location as a function of gas chemistry changing from nonequilibrium to equilibrium. The second occurrence ( $4.0 > V_\infty > 3.1$  km/s,  $25 > h > 2$  km) results from the translation in the sonic-line location as a function of decreasing flow enthalpy in an equilibrium gas chemistry regime.

The occurrence of a static instability at two different times during entry was considered a serendipitous event for CA. The

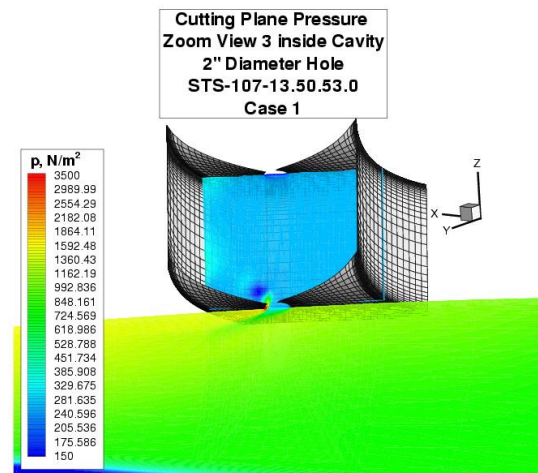


Figure 5: View of idealized, vented chamber under breach on wing leading edge with pressure distributions in cut plane spanning exterior and interior domains for Columbia Accident Investigation.

static instability provides a clearly defined signal on the accelerometers to validate the simulation. Furthermore, the effect is a sensitive function of the computed pressure distributions as a function of gas chemistry; consequently a prediction of the event presents an important accomplishment in the validation of CA. The validation payoff came after a successful mission in July 1997 as shown in Figure 4 where the predicted accelerations using the CA database are compared to the flight accelerometer measurements. While there is a slight shift in velocity space between the predicted and measured onset of the static instability its occurrence is clearly evident. More detailed post-flight evaluations are available in Reference [18].

#### Columbia Accident Investigation (Reference [16])

STS-107, Columbia, and its crew of seven astronauts were lost on entry on February 1, 2003. According to the Columbia Accident Investigation Board (CAIB) report [14], it "re-entered Earth's atmosphere with a pre-existing breach in the leading edge of its left wing in the vicinity of Reinforced Carbon-Carbon (RCC) panel 8. This breach, caused by the foam strike on ascent, was of sufficient size to allow superheated air (probably exceeding 5,000 degrees Fahrenheit) to penetrate the cavity behind the RCC panel." In the weeks immediately following the accident this root cause was suggested by films of the foam strike but intensive investigation was required to build evidence that the timeline of various recorded events was consistent with an initial breach condition. To this end, a matrix of CA solutions using a 5-species air model was generated to provide a nominal baseline for assessing various breach sizes and locations.

A baseline solution for CFD Point 1 (Mach 24) in the STS-107 accident investigation was modified to include effects of holes through the leading edge into a vented cavity. The simulations were generated relatively quickly and early in the investigation (March 28, 2003 to April 10, 2003) by making simplifications to the leading edge cavity geometry using a grid morphing tool that had originally been developed to do quick assessments of RCS jet locations. These simplifications in the breach simulations enabled: (1) a very quick grid generation procedure; (2) high fidelity corroboration of jet physics with internal surface impingements ensuing from a breach through the leading edge, fully coupled to the external shock layer flow at flight conditions; and (3) mass and energy inflow rates into the wing as a

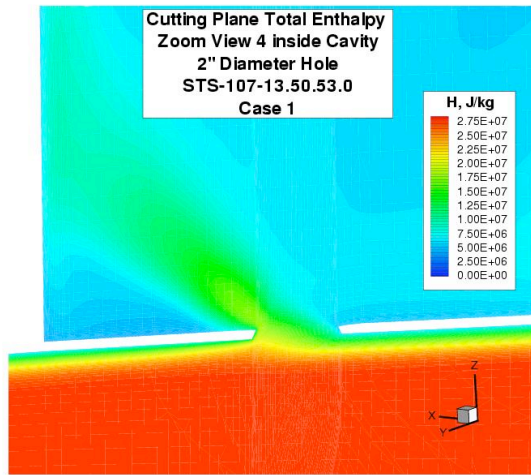


Figure 6: Total enthalpy in vicinity of breach indicating level of ingestion of the external boundary layer.

function of breach size to feed other analyses.

Figure 5 shows the pressure distributions in a cut plane that is approximately orthogonal to the wing leading edge over a two-inch hole into the wing. The cut plane extends into a vented chamber within the wing into which flow hot gasses from the external shock layer. The grid used to define the walls of the chamber are shown as well. These simulations provided early evidence that the flow through a two-inch diameter (or larger) breach enters the cavity with significant retention of external flow directionality. As seen in Figure 6 a normal jet directed into the cavity was not an appropriate model for these conditions at CFD Point 1 (Mach 24). The breach diameters were of the same order or larger than the local, external boundary-layer thickness. High impingement heating and pressures on the downstream lip of the breach were also computed. It is likely that hole shape would evolve as a slot cut in the direction of the external streamlines. In the case of the six-inch diameter breach the boundary layer is fully ingested.

The role of CA in mission support has been profoundly advanced as a consequence of the accident investigation. Prior to Columbia there was no available matrix of CA solutions spanning the trajectory. Post Columbia missions utilize a repository of flowfield solutions in standby mode for use in damage assessment. CA teams are on call to morph damage sites into archived nominal solutions and provide data to complement the suite of engineering tools that are the backbone of the damage assessment process. Morphed solutions are completed within 18 hours of the delivery of the damage shape and location.

The role of CA in the Damage Assessment Team has also accentuated deficiencies in the current SOA. CA cannot predict transition to turbulent flow, either naturally occurring or resulting from trips in the boundary layer as with protruding gap fillers. Rather, it provides the boundary layer characteristics as a function of location on the vehicle and trajectory point in the atmosphere to empirical prediction tools for transition. CA is not coupled to the thermal response of the vehicle. It typically uses a radiative equilibrium wall boundary condition to define surface temperature. It cannot account for significant conduction relief through the surface that occurs at the sharp ridges of cavities and protuberances. Within a cavity, CA does not routinely use radiation view factors to modify thermal boundary conditions within a cavity. Finally, the coupled multiphysics simulations required to simulate hole growth, starting from a crack

in which continuum approximations are invalid are not yet handled by CA. Consequently, the primary CA deliverable in the damage assessment process is a heating bump factor associated with the effect of a damage configuration relative to a nominal configuration. Other effects are approximated by more rapid running engineering tools.

## State-of-Art (SOA)

### CA Codes

**Continuum, Structured Grid:** The main CA codes in NASA for parallel, multiblock, continuum flow analyses are Langley Aerothermodynamic Upwind Relaxation Algorithm (LAURA)[12, 19] and Data Parallel Line Relaxation (DPLR)[40] for external flows and VULCAN[38] for internal, scram-jet flows. These codes employ finite-volume formulations of the Reynolds-averaged Navier-Stokes equations with upwind discretizations for inviscid flux (quasi-one-dimensional reconstruction) and central differences for viscous flux. They employ both point-implicit and line-implicit relaxation strategies. VULCAN also has options to engage a space marching algorithm where appropriate in a flow path. Alignment of the structured grid with the captured bow shock is a critical element for simulation quality. LAURA has used a quasi-one-dimensional grid adaptation strategy since its inception in 1987 that automatically aligns the grid with the bow shock during the computation and resets the near-wall mesh spacing to attain a cell-Reynolds number of order 1. DPLR adopted a similar adaptation strategy during the post-Columbia Return to Flight era. LAURA and DPLR are usually run in tandem to supply aerothermodynamic environments for projects like Crew Exploration Vehicle (CEV) design and planetary exploration. A matrix of needed cases is divided between teams running each code using occasional overlap of coverage to provide independent checks of computed environments. On rare occasion this practice has flushed out problems when results disagree - a process that benefits both codes in an environment where the suite of models and flow conditions are varied and complex. The practice also acknowledges that ground-based experimental validation is more difficult to obtain in these high temperature, nonequilibrium environments; shock tunnels, expansion tubes, and arc jets all do imperfect simulations of the intended design space and are more dependent on CA for extrapolation to flight.

**Continuum, Unstructured Grid:** Unstructured grids provide the greatest flexibility to resolve complex flowfields. However, in the hypersonic regime, use of simplex tetrahedral elements with SOA flux reconstruction corrupts the shock capturing and the stagnation region heating.[15] Still, unstructured grids are making inroads into CA for three reasons. First, it is easier to achieve load balancing on massively parallel architectures without being constrained by structured-block boundaries. Second, mixed-element formulations (ability to use tetrahedra, pyramids, prisms, and hexahedra) enable structured grids to be used where required for accuracy. Third, there is expectation that algorithm advances will remove semi-structured requirements thus opening the way for orders-of-magnitude faster grid generation and adaptation for complex configurations with moving boundaries as compared to structured grid methods. FUN3D[2] and US3D[31] are mixed element, finite-volume solvers of the Euler and Navier-Stokes equations. US3D and DPLR share a similar development history. FUN3D was developed independently of LAURA but a suite of modules have been added to FUN3D to synthesize all of the gas physics models in LAURA and VULCAN for thermodynamics, transport properties, chemical kinetics, and thermal relaxation. The turbulence models in VULCAN have also been added to FUN3D.

**Non-continuum:** Heating analyses at the lower densities of transitional rarefied flow require the Direct Simulation Monte Carlo (DSMC) technique developed by Bird[4]. DSMC simulates gas flows by modeling the motion and collisions of millions of representative molecules based on the kinetic theory of gases. The DSMC technique captures the non-equilibrium in translational and internal degrees of freedom, which is strongly evident in most rarefied flows, and uses phenomenological models to describe the inelastic collisions that may occur between gas molecules and surfaces. The DSMC simulations used in NASA include the DS2V[5] and DS3V[6] programs of Bird and the DAC[28] program of LeBeau. These codes provide both time accurate unsteady flow and time-averaged flow simulations. Molecular collisions are simulated with the variable hard sphere (VHS) molecular model. Energy exchange between the translational and internal modes is controlled by the Larsen-Borgnakke statistical model[7].

### Thermo-chemical models

Chemical kinetic models in LAURA and DPLR utilize the compilation of rate constants assembled by Park predominantly derived from shock-tube experiments. The effects of thermal non-equilibrium on reaction rates are approximated by Park's two-temperature model in a simple, ad-hoc fashion calibrated to shock tube measurements.[32] The two-temperature model assumes that the distribution of energy in vibrational and electronic modes can be defined by a Boltzmann distribution at temperature  $T_v$ . Exchange of energy between rotational-translational modes and vibrational-electronic modes include: (1) vibrational relaxation through collisions with heavy particles as correlated by Millikan and White and modified by Park at high temperatures; (2) preferential and non-preferential models for dissociation defining the vibrational energy content of molecules as they are created and destroyed; (3) losses due to electron-impact ionization; and (4) electronic-translational relaxation.[19] The impact of thermal nonequilibrium on a hypersonic flow is to retard dissociation behind strong shocks, thus raising the shock layer temperature and increasing shock stand-off distance. These effects in turn have a modest influence on pressure distributions but have a very large effect on radiative energy transfer across the shock layer. Recall that modest influence on pressure distributions acting over large areas can have significant influence on pitching moment coefficients.

### Catalysis

Aerothermodynamic simulation tools for surface catalysis of air assume homogeneous recombination of atomic oxygen to molecular oxygen and atomic nitrogen to molecular nitrogen. All charged particles are de-ionized at the surface. Nitric oxide (NO) is not produced at the surface; consequently, the gradient of mole fraction of NO at the surface is set to zero. Curve fits of catalytic efficiency  $\gamma_r$  as a function of surface temperature for pure oxygen and pure nitrogen are compiled for several TPS materials and coatings.[34, 35] Surface catalysis of CO<sub>2</sub> in the Martian atmosphere is generally assumed to be fully catalytic, the most conservative approximation to maximize heating. Another approximation for the Martian atmosphere is to assume that atomic oxygen is fully catalysed to molecular oxygen and all other species are treated as non-catalytic. Effects of finite number of surface adsorption sites, non-homogeneous recombination, and competition for adsorption sites are not included in standard models used in either LAURA or DPLR within NASA.

### Ablation

CMA and FIAT are state-of-art material response codes for ablation modeling used in NASA.[13] The infrastructure is in

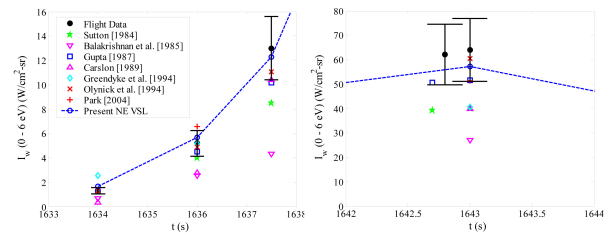


Figure 7: Comparison of simulations of radiative intensity in the range 0.2 to 6.2 eV with measured FIRE II total radiometer data.

place for coupling structured CFD and FIAT but only preliminary validation on simple problems exists at present. The Galileo and Stardust missions provide some flight data for recession as a function of time. Time dependent shape change is not fully automated at present nor does it model the surface roughness that may ensue from uneven surface response.

### Radiation

The current state-of-art in radiation modeling within NASA is best summarized by Hash et. al.[26] and Johnston[27]. Line-by-line (LBL) and smeared rotational bands (SRB) integrations are used to obtain radiation intensity along a line of sight. Tangent slab approximations are generally applied in order to simplify integration to a single line of sight orthogonal to the surface of a blunt body. Loose coupling of the radiative energy transfer to the conservation equations for mass, momentum, and energy is implemented in a sequential manner, requiring 5 to 10 sequential passes to converge the radiative flux to the wall. The time to complete a radiation calculation is 1 to 4 orders of magnitude longer than the time to complete a flow solve. This wide variation is a strong function of the spectral resolution and coarsening of the flow grid to the radiation spatial grid. The FIRE II flight data (total heating, radiative heating over the range 0.23 to 4  $\mu\text{m}$  (0.31 to 5.4 eV), and spectral radiometer over the range 0.3 to 0.6  $\mu\text{m}$ ) taken on May 22, 1965 remain the touchstone for validation of air radiation simulations.[29, 10] SOA simulation tools in NASA agree with total radiometer data within experimental uncertainty in both the nonequilibrium and equilibrium flight regimes. (See Figure 7) However, there remains some ambiguity in calibration of the suite of energy exchange models that lead to acceptable agreement with the data for this single flight.

### Turbulence models

Turbulence models are critically important for the simulation of mixing in scramjet engines.[38] VULCAN has options for  $k - \epsilon$  models, Wilcox's  $k - \omega$  model[39], and Menter's[30]  $k - \omega$  (baseline and Shear Stress Transport (SST)) model. Options for an explicit algebraic Reynolds Stress model[1] are available in VULCAN and FUN3D. LAURA and DPLR typically apply Wilcox's  $k - \omega$  model and Menter's  $k - \omega$  SST model. Compressibility corrections are required in hypersonic applications.[41, 33] In cases without separation LAURA will typically use simple algebraic turbulence models[11, 3].

### Spacecraft - Tether - Ballute System Simulation

A simulation of a spacecraft - tether - ballute system using the unstructured grid, Navier-Stokes flow solver FUN3D is presented in Figs. 8 - 11. The system is chosen as a current example because it is so far "out of the box" of typical applications and it exhibits several challenges facing CA today.

The ballute has a 52 m ring diameter and 13 m cross-sectional diameter. Conditions of the simulation are for a Titan Organics Explorer with velocity equal to 8550 m/s and density equal to  $1.9 \cdot 10^{-7} \text{ kg/m}^3$ . [24, 25] All surface temperatures are set to a constant value equal to 500 K. The gas model includes molecular nitrogen and atomic nitrogen in thermochemical nonequilibrium. The towing spacecraft is a Pathfinder shape – 70 deg spherically capped cone with a 6 m base diameter. The simulation domain encompasses a 90 degree wedge about the system axis. The simulation assumes symmetric flow with four 0.3 m diameter compressive tethers attached to the toroid so that the leading edge of the tether is tangent to the toroid outer surface. A compressive tether is a flexible cylinder which can be inflated to withstand compressive loads and is used to position the toroid in space prior to entry. At present, only a continuum simulation is enabled. Flow over the compressive tethers is deep in the transitional flow domain in which the validity of Navier-Stokes analyses is inaccurate. Consequently, an independent analysis of the tether using DSMC is required. Ideally, a fully coupled continuum - rarefied analysis would be brought to bear on this complex system of disparate length scales.

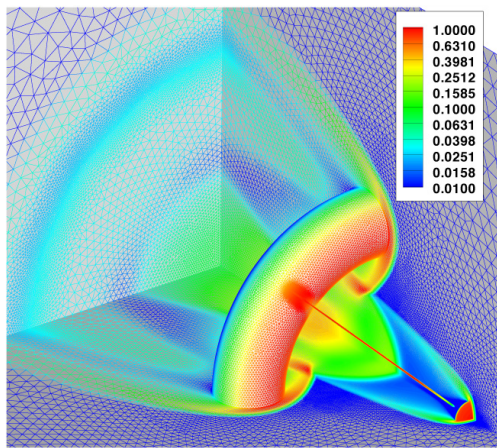


Figure 8: Unstructured grid used in simulation of spacecraft - tether - ballute system. Colors correspond to pressure levels nondimensionalized by  $\rho_\infty V_\infty^2$ .

The quarter domain in Figure 8 is discretized with 992,102 nodes. Flow over the spacecraft is in a merged layer, transitional regime. The Knudsen number based on spacecraft diameter is approximately 0.057. Flow over the ballute is still in a transitional regime, but is closer to the continuum domain than the towing spacecraft. The Knudsen number based on ballute cross-sectional diameter is 0.026. The cell Reynolds number at the ballute surface is approximately 0.2 with approximately 20 nodes extending across the shock layer and 3 to 4 nodes extending across the “inviscid” portion of the shock layer. The largest mesh height stretching factor is approximately 2.0 and it occurs where the advancing front of the boundary domain over the ballute meets the isotropic grid away from the solid surface. In the domain where the tether is directly exposed to the free stream the Knudsen number based on tether diameter is approximately 0.88, placing it near the free molecular limit of the transitional flow regime. Near wall grid resolution is well within accepted norms for simulation of surface heating. Results presented herein with FUN3D should be considered qualitative at present. Stretching factors of two in the merged layer exceed accepted structured grid metrics and there is lack of validation or grid convergence study in this domain. Furthermore, issues remain regarding ability to compute heat transfer with

high aspect ratio, tetrahedral cells in the boundary layer within the stagnation region of a blunt body in hypersonic flow. [22]

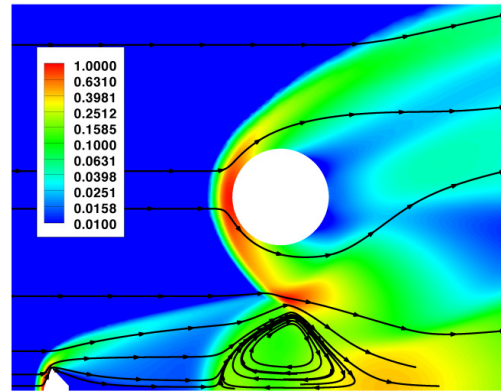
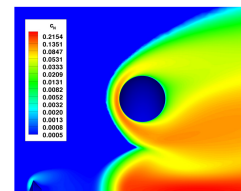
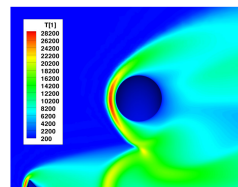


Figure 9: Pressure contours and streamlines in symmetry plane. Colors correspond to pressure levels nondimensionalized by  $\rho_\infty V_\infty^2$

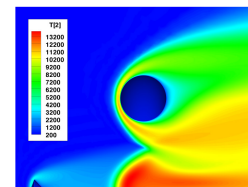
Pressure distributions in the plane of symmetry away from the tether are presented in Figure 9. The extent of reverse flow through the wake core is in good agreement with the earlier LAURA solution [17] that did not include the tether. The flow is nearly frozen chemically, consistent with the spacecraft Knudsen number, as indicated in Figure 10(a). It is not until the flow crosses the ballute bow shock or enters the recirculating flow driven by the converging shocks in the core of the toroid that residence times in a high temperature domain are long enough to enable dissociation. In like manner, thermal nonequilibrium is evident in Figure 10. Vibrational temperatures lag translational temperatures by nearly 20,000 K at the shock front but then exceed translational temperature in the recirculating core. A front view of the entire system, including grid, pressure, and



(a) Atomic nitrogen mass fraction



(b) Translational temperature



(c) Vibrational temperature

Figure 10: Chemical and thermal state in symmetry plane.

heating is presented in Figure ???. Surface grid in the vicinity of the attachment point is clustered to pick up details of the interaction. A high pressure and heating occurs on the ballute sur-

face associated with the shock over the tether interacting with the bow shock over the ballute as seen in Figure 11. Surface streamlines show that the attachment line is pulled further outboard toward the tether attachment point. The heating rate on the ballute surface is approximately 70% larger than nominal rates on the attachment line away from the tether. Pressures too are greater than nominal values on the attachment line due to the focusing of the ballute shock - tether shock interaction. In reality, significant deformation of this system, possibly unsteady, would be expected.

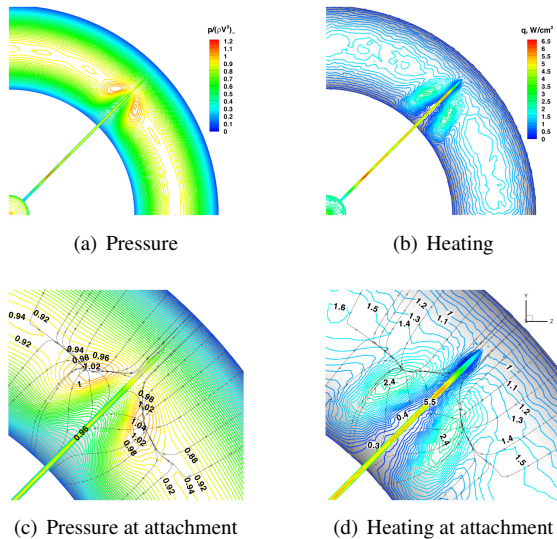


Figure 11: Front view of surface pressure and heating.

### View Forward

In the view forward for CA simulation there are still significant advances in capability required. Many of these challenges to advance the SOA have been identified in previous examples. In some instances, the capabilities have been demonstrated on simple geometries but have not made their way to production CA. Some of the most notable remaining challenges are to enable:

- (1) Accurate shock capturing and stagnation region heating on high aspect ratio, tetrahedral grids This advance probably requires flux reconstruction algorithms that are inherently multidimensional. Advances here greatly enhance the possibility of fully automated grid adaptation on complex, hypersonic configurations without restriction to prismatic elements. A long term goal here is to be able to start a simulation on a quickly generated, reasonable grid that automatically refines to achieve user specified grid convergence levels for key design parameters.
- (2) Large Eddy Simulations (LES) in production CA Requires development of low dissipation schemes and probably higher-order accurate schemes. Advances here may be expected to greatly reduce uncertainties in prediction of base drag effect on blunt bodies at Mach numbers below 5. Also promises to improve turbulence simulations in more complex environments of separated flow and shock - boundary-layer interactions. It is expected that direct numerical simulations (DNS) on canonical problems will guide the development of sub-grid models required here.
- (3) Automated prediction of transition to turbulence and re-laminarization in production CA Overly conservative prediction of transition to turbulence costs weight in thermal protection system mass. On STS-114 the level of uncertainty was

sufficient to order removal of exposed gap fillers lest early transition to turbulence ensue and a turbulent wedge of heating wash over the wing leading edge.

(4) Fully coupled, multi-physics simulations These multi-physics elements include: unsteady deformation, thermal response of structure, ablation, radiation, rarefied and continuum flow domains, and Magneto-hydro-dynamics (MHD). The challenges here exist in both improving efficiencies of the component physics simulations and in time-accurate, viscous grid movement to accommodate shape change due to ablation or structural deformation.

(5) Facility simulation in the code validation process Ground-based tests provide the best opportunity to measure boundary conditions and probe the flowfield with sufficient detail to validate physical models. However, the facilities are not perfectly quiet and often the flows are neither perfectly uniform nor perfectly steady. As enthalpies are increased flow quality and test times become more problematic. Recent efforts by Candler et al. [9] underscore the proposition that future code validation tests will require more complete simulation of the facility flow in addition to simulation around models.

### Conclusions

Code verification and validation are required for acceptance of any CFD simulation tool. Because ground-based validation has often been more difficult in the hypersonic domain the opportunity to resolve highly visible problems in flight data analyses have helped grow the credibility of CA. CA's role in understanding the Space Shuttle pitching moment anomaly observed in the first shuttle flight, its prediction of a static instability for Mars Pathfinder, and its use for damage assessment in both the Columbia accident investigation and post-Columbia mission-support have all served to advance its credibility to the wider community of engineers.

Current state-of-art in "production" codes used in NASA for CA is described. In the view forward, several current challenges in computational fluid dynamics and aerothermodynamics for hypersonic vehicle applications are noted. An example simulation dealing with hypersonic flight of an inflated ballute trailing a planetary probe in the Titan atmosphere is presented to illustrate current capabilities and limitations.

### References

- [1] Abid, R., Rumsey, C. and Gatski, T. B., Prediction of nonequilibrium turbulent flows with explicit algebraic turbulence models, *AIAA J.*, **33**.
- [2] Anderson, W. K. and Bonhaus, D. L., An implicit upwind algorithm for computing turbulent flows on unstructured grids, *Comp. and Fluids*, **23**, 1994, 1-21.
- [3] Baldwin, B. S. and Lomax, H., Thin Layer Approximation and Algebraic Model for Separated Turbulent Flows, *AIAA Paper 78-257*, 1978.
- [4] Bird, G. A., *Molecular Gas Dynamics and the Direct Simulation of Gas Flows*, Clarendon Press, Oxford, 1994.
- [5] Bird, G. A., *Visual DSMC Program for Two-Dimensional and Axially Symmetric Flows*, The DS2V Program User's Guide, Version 2.1, 2003.
- [6] Bird, G. A., *Visual DSMC Program for Three-Dimensional Flows*, The DS3V Program User's Guide, Version 2.2, 2006.

- [7] Borgnakke, C. and Larsen, P. S., Statistical collision model for monte carlo simulation of polyatomic gas mixture, *J. Comput. Phys.*, **18**, 1975, 405–420.
- [8] Braun, R. D., Powell, R. W., Engelund, W. C., Gnoffo, P. A., Weilmuenster, K. J. and Mitcheltree, R. A., Mars pathfinder six-degree-of-freedom entry analysis, *J. Spacecraft and Rockets*, **32**, 1995, 993–1000.
- [9] Candler, G. V., Nompelis, I., Druguet, M.-C., Holden, M. S., Wadhams, T. P., Boyd, I. D. and Wang, W.-L., Cfd validation for hypersonic flight - hypersonic double-cone flow simulations, AIAA Paper 2002–0581, 2002.
- [10] Cauchon, D. L., Radiative Heating Results from the FIRE II Flight Experiment at a Reentry Velocity of 11.4 Kilometers per Second, NASA TM X–1402, 1967.
- [11] Cebeci, T. and Smith, A. M. O., A Finite-Difference Method for Calculating Compressible Laminar and Turbulent Boundary Layers, *Journal of Basic Engineering*, 523–535.
- [12] Cheatwood, F. M. and Gnoffo, P. A., User’s Manual for the Langley Aerothermodynamic Upwind Relaxation Algorithm (LAURA), NASA TM 4674, 1996.
- [13] Chen, Y.-K. and Milos, F. S., Ablation and Thermal Analysis Program for Spacecraft Heatshield Analysis, *J. Spacecraft and Rockets*, **36**, 1999, 475–483.
- [14] Gehman Jr., H. W. and et. al., Columbia Accident Investigation Board, Report Volume I, NASA, August 2003, p12.
- [15] Gnoffo, P. A., Simulation of Stagnation Region Heating in Hypersonic Flow on Tetrahedral Grids, AIAA Paper 2007-3960, 2007.
- [16] Gnoffo, P. A. and Alter, S. J., Simulation of flow through breach in leading edge at mach 24, AIAA Paper 2004-2283, 2004.
- [17] Gnoffo, P. A. and Anderson, B. P., Computational analysis of towed ballute interactions, AIAA Paper 2002-2997, 2002.
- [18] Gnoffo, P. A., Braun, R. D., Weilmuenster, K. J., Mitcheltree, R. A., Engelund, W. C. and Powell, R. W., Prediction and validation of mars pathfinder hypersonic aerodynamic data base, AIAA Paper 98–2445, 1998.
- [19] Gnoffo, P. A., Gupta, R. N. and Shinn, J. L., Conservation equations and physical models for hypersonic air flows in thermal and chemical nonequilibrium, NASA TP 2867, 1989.
- [20] Gnoffo, P. A., Weilmuenster, K. J., Braun, R. D. and Cruz, C. I., Influence of sonic-line location on mars pathfinder probe aerothermodynamics, *J. Spacecraft and Rockets*, **33**, 1996, 169–177.
- [21] Gnoffo, P. A., Weilmuenster, K. J., Hamilton, H. H., Olynick, D. R. and Venkatapathy, E., Computational aerothermodynamic design issues for hypersonic vehicles, *J. Spacecraft and Rockets*, **36**, 1999, 21–43.
- [22] Gnoffo, P. A. and White, J. A., Computational aerothermodynamic simulation issues on unstructured grids, AIAA Paper 2004-2371, 2004.
- [23] Griffith, B. J., Maus, J. R. and Best, J. T., Explanation of hypersonic longitudinal stability problem – lessons learned, NASA CP CP-2283, 1983.
- [24] Hall, J. L., A review of ballute technology for planetary aerocapture, IAA Paper L-1112, 2000.
- [25] Hall, J. L. and Le, A., Aerocapture trajectories for spacecraft with large towed ballutes, AAS Paper 01-235, 2001.
- [26] Hash, D. B., Olejniczak, J., Wright, M., Prabhu, D., Pulsonetti, M., Hollis, B., Gnoffo, P., Barnhardt, M., Nompelis, I. and Candler, G., FIRE II Calculations for Hypersonic Nonequilibrium Aerothermodynamics Code Verification: DPLR, LAURA, and US3D, AIAA Paper 2007-0605, 2007.
- [27] Johnston, C. O., Hollis, B. R. and Sutton, K., Nonequilibrium Stagnation-Line Radiative Heating for Fire II, AIAA Paper 2007-3908, 2007.
- [28] LeBeau, G. J., A User Guide for the DSMC Analysis Code (DAC) Software for Simulating Rarefied Gas Dynamic Environments, Revision DAC97-G 4674, NASA Johnson Space Center, 2002.
- [29] Lewis Jr., J. H. and Scallion, W. I., Flight Parameters and Vehicle Performance for Project FIRE Flight II, Launched May 22, 1965, NASA TN D–3569, 1966.
- [30] Menter, F. R., Improved two-equation  $k-\omega$  turbulence model for aerodynamic flows, NASA TM 103975, 1992.
- [31] Nompelis, I., Drayna, T. W. and Candler, G., A Parallel Unstructured Implicit Solver for Hypersonic Reacting Flow Simulation, AIAA Paper 2005-4867, 2005.
- [32] Park, C., *Nonequilibrium Hypersonic Aerothermodynamics*, John Wiley & Sons, Inc., 1990.
- [33] Sarkar, S., Erlebacher, G., Hussaini, M. Y. and Kreiss, H. O., The analysis and modeling of dilational terms in compressible turbulence, ICASE Report 89-79, 1989.
- [34] Stewart, D. A., Determination of Surface Catalytic Efficiency for Thermal Protection Materials – Room Temperature to Their Upper Use Limit, AIAA Paper 96–1863, 1996.
- [35] Stewart, D. A., Surface Catalysis and Characterization of Proposed Candidate TPS for Access-to-Space Vehicles, NASA TM 112206, 1997.
- [36] Venkatapathy, E., Rakich, J. V. and Tannehill, J. C., Numerical solution of space shuttle orbiter flow field, AIAA Paper 82–0028, 1982.
- [37] Weilmuenster, K. J., Gnoffo, P. A. and Greene, F. A., Navier-Stokes Simulations of Orbiter Aerodynamic Characteristics Including Pitch Trim and Bodyflap, *J. Spacecraft and Rockets*, **31**, 1994, 355–366.
- [38] White, J. A. and Morrison, J. H., A pseudo-temporal multi-grid relaxation scheme for solving the parabolized Navier-Stokes equations, AIAA Paper 99–3360, 1999.
- [39] Wilcox, D. C., *Turbulence Modeling for CFD*, 2nd Edition, DCW Industries, Inc., La Cañada, CA, 1998.
- [40] Wright, M. J., Candler, G. V. and Bose, D., Data-parallel line relaxation method for the navier-stokes equations, *AIAA J.*, **36**, 1998, 1603–1609.
- [41] Zeman, O., Dilational dissipation: The concept and application in modeling compressible mixing layers, *Physics of Fluids*, **2**.